Transverse oscillations in a single-layer dusty plasma under microgravity

Bin Liu,[1] J. Goree,[1] V. E. Fortov,[2] A. M. Lipaev,[2] V. I. Molotkov,[2] O. F. Petrov,[2] G. E. Morfill,[3] H. M. Thomas,[3] H. Rothermel,[3] and A. V. Ivlev[3]
[1]*Department of Physics and Astronomy, The University of Iowa, Iowa City, Iowa 52242, USA*
[2]*Joint Institute for High Temperatures, Russian Academy of Sciences, 127412 Moscow, Russia*
[3]*Max-Planck-Institut für extraterrestrische Physik, 85748 Garching, Germany*

(Received 8 April 2009; accepted 23 July 2009; published online 13 August 2009)

A single-layer suspension of microparticles was formed in a plasma under microgravity conditions. This single layer is confined at a void boundary by a balance of ion drag and electric forces, where the ion flow velocity is much slower than in the sheath of laboratory plasmas. Using a high-resolution camera that allows measurements of velocities at a low level, the microparticle kinetic temperature was found to be close to that of the neutral gas. The random motion transverse to the single layer was found to have oscillations of the form expected for harmonic oscillators driven by white noise. The driving of the oscillation is mostly attributed to the Brownian motion of neutral atoms, while the damping is mostly due to neutral gas friction. An observed resonance frequency of 25 s^{-1} allows us to quantify the electric and ion drag forces as being in the range of $0.2–0.4 m_p g$, where m_p is the microparticle mass and g is the acceleration of gravity on Earth's surface. No signature of wave dispersion was detected for this experiment with neon at a pressure of 0.12 Torr. © *2009 American Institute of Physics*. [DOI: 10.1063/1.3204638]

I. INTRODUCTION

A dusty plasma (also termed as complex plasma) is an ionized gas containing electrons, ions, and small particles of solid matter, i.e., microparticles. The dynamics of the microparticles are of particular interest in astrophysics because of objects such as planetary rings, comet tails, and nebulae that include dusty plasma.[1] Dusty plasma is also of interest for industrial processing of semiconductor chips.[2] Additionally, dusty plasma has uses in fundamental physics because the microparticles in plasma self-organize in equilibrium positions that mimic crystalline and liquid structures in condensed matter physics.[3–22] Experiments with dusty plasmas are often done by introducing microparticles into a glow discharge plasma, where they became electrically charged and confined in a suspension. The charge is usually negative when the surrounding plasma consists of positively charged ions and negatively charged electrons. The charge can be as large as thousands of elementary charges for particles larger than a micron. Here, we will study oscillations of microparticles in a suspension consisting of a single layer.

The experiment reported here was performed under microgravity conditions. One advantage of performing experiments with microgravity is the ability to reduce the anisotropy and nonequilibrium effects arising from high velocity ion flow. In most ground-based experiments, due to gravity, microparticles are suspended in a sheath between the main plasma and electrode. In this sheath, electric fields are strong, and they drive ion flows that provide a source of energy for microparticles. Under microgravity conditions, microparticles are suspended in the main plasma, where the electric field and the resulting ion velocity are much lower, so that we can achieve conditions that are less anisotropic and more nearly like equilibrium conditions.

A. Forces acting on a single microparticle

Many forces can act on a microparticle, most importantly an electric force $Q\mathbf{E}$ due to an electric field $\mathbf{E}$. Additional forces include gravity, ion drag, gas friction, and the thermophoretic force.

The forces we have listed above can be classified according to whether they are conservative. Gravity is of course a conservative force. The electric force is a conservative force as well if the charge is constant. (In a dusty plasma, the charge can vary with local conditions[23] such as ion velocity, although this can be a small effect, if the microparticles do not move a great distance.) Gas drag and ion drag vary with velocity and therefore are nonconservative forces, as will be discussed later.

Gravity is often a dominant force for microparticles larger than a micron in ground-based experiments. The effects of gravity can be mostly eliminated by performing the experiment in free fall; this has been done in sounding-rocket flights,[24] space stations,[25–28] and parabolic flights of aircraft.[29]

The electric force QE on a microparticle arises from two kinds of electric fields. First, in the absence of other microparticles, there is a natural electric field due to ambipolar transport in the plasma. Second, when there are many microparticles, they also experience a mutual repulsion due to their negative charges, which can result in wave propagation.

The gas drag force is the resistance experienced by a microparticle moving through a gas. For a microparticle with a size smaller than the gas mean-free path, and with a velocity slower than gas molecule's thermal velocity, gas drag is modeled by the Epstein expression[30,31]

$$F_{\text{gas}} = 4\pi\delta N m \bar{c} r_p^2 V/3, \tag{1}$$

where N, m, and $\bar{c}$ are the number density, mass, and mean thermal speed of gas atoms, respectively, r_p is microparticle radius, and V is microparticle's velocity relative to the gas. The coefficient δ depends on how gas molecules scatter from the microparticle's surface.[30] Dividing F_{gas} by the microparticle's momentum $m_p V$ yields the Epstein damping rate

$$\nu_E = 4\pi\delta N m \bar{c} r_p^2/3m_p, \tag{2}$$

which is independent of the velocity of the microparticle. Here, m_p is the microparticle's mass. We expect any fluctuations in microparticle motion to be damped away for times longer than ν_E^{-1}.

Neutral gas atoms apply drag not only to microparticles but also to ions. When the ion-neutral mean-free path is smaller than the dimensions of the main plasma, as in our experiment, ion motion will be mobility limited, with a drift velocity that depends on electric field and a mobility coefficient. At low electric fields, ion velocity scales linearly with electric field. A typical mobility-limited ion velocity in the main plasma of a gas discharge is about 10^4 cm/s [with a mobility coefficient of about 2×10^4 cm^2 V^{-1} s^{-1} (Ref. 32) in a 1 V/cm electric field in neon gas at a pressure of 0.1 Torr]. This ion velocity is six orders of magnitude higher than the microparticle velocity, which is typically 0.01 cm/s (for 10 μm diameter particles with a kinetic temperature of 300 K). At higher electric fields, the scaling of ion velocity with electric field is weaker than linear.[32]

Ion drag is a force of an electrical nature that is imparted onto microparticles by momentum transfer from ion flows.[33–35] Ions, accelerated by electric field in plasma, exert a force on a microparticle that is in the direction of ion flow. The magnitude of the ion drag force F_{ID} depends on the flow speed, which ultimately depends on the electric field. Near the center of the plasma, where the electric field and ion flow velocity are smallest, F_{ID} scales mostly linearly with ion velocity and therefore with electric field. Under these circumstances, F_{ID} is almost proportional to electric field. However, at higher electric fields, as found for example near the plasma-sheath edge, the ion velocity is higher, and the scaling of F_{ID} varies nonlinearly with ion velocity with a maximum at approximately the ion thermal velocity.

Although the ion drag force varies with the relative velocity of microparticles and ions, this force can be nearly conservative. There are two reasons for the nearly conservative nature of the ion drag force for conditions as in the experiment reported here. First, near the low-field conditions near the plasma center, the ion drag force is nearly proportional to the electric field as explained above, so that it is nearly conservative. Second, the ion drag force is almost constant for small-amplitude motion of microparticles. This is true because the ion velocity is typically six orders of magnitude higher than the microparticle velocity. As a microparticle moves about randomly, toward, and then away from the source of ion flow, the relative velocity remains nearly constant, and therefore the ion drag force also remains nearly constant. When the ion drag force is nearly conservative, as it is in the experiment reported here, the primary nonconservative force is the gas drag force.

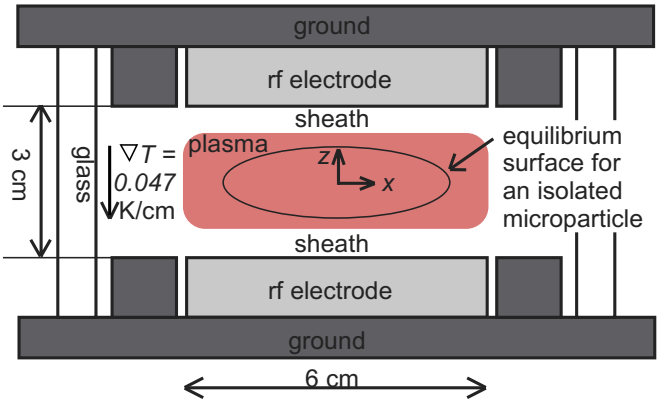

FIG. 1. (Color online) Side-view cross section of the PK-3 Plus vacuum chamber. Neon plasma is generated by applying rf voltages to a pair of parallel-plate electrodes. Microparticles are introduced by a dispenser and viewed from the side by video cameras, not shown here. The microparticles are charged and confined stably. A single isolated microparticle would rest anywhere on an equilibrium surface where the net force is zero.

B. Voids in dusty plasma

A void is a microparticle-free region surrounded by a suspension of microparticles. Voids are often observed in three-dimensional (3D) suspensions[24,26–29,36–40] in a gas-discharge plasma, especially those that are powered by capacitively coupled radio frequency (rf) voltages applied to a pair of electrodes, as in Fig. 1. Voids were reported first in ground-based experiments with carbon particles of submicron size,[36] and then in microgravity experiments performed in a sounding rocket,[24] parabolic airplane flights,[29] and the International Space Station (ISS). The ISS experiments were performed using the PKE-Nefedov instrument,[26,28] and more recently the PK-3 Plus instrument.[27]

To understand the mechanism for generating voids, we review ambipolar transport in a gas-discharge plasma in the absence of microparticles. Electrons are accelerated by electric fields, and they ionize a gas molecule, releasing a positive ion and a negative electron. Due to its lower mass, an electron would tend to escape more rapidly, so that a positive space charge develops in the plasma center. A steady state develops with an electric field that (averaged over time) points outward. An outward flow of ions is driven by this electric field.

If we now insert a single microparticle into this plasma, and it acquires a negative charge, it will experience two forces of an electrical nature: the electric force and the ion drag force. The electric force points inward toward the plasma center, while the ion drag force is in the opposite direction, away from the plasma center. This is so because the ion drag force is always in the direction of ion flow, which for positively charged ions is always in the same direction as the electric field.

In equilibrium, an isolated microparticle will come to

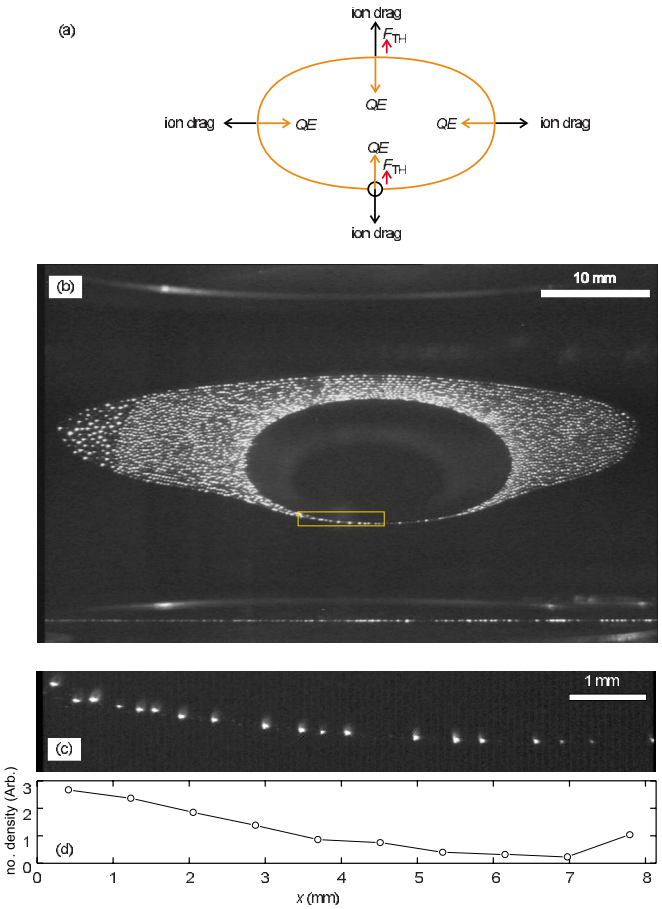

FIG. 2. (Color online) (a) Sketch of the force balance for microparticle confinement. At equilibrium, under microgravity conditions, microparticles experience electric and ion drag forces that are opposite and are almost equal, as well as a small thermophoretic force F_{TH} due to a temperature gradient. The electric field drives an outward ion flow. (b) A cross section of the entire microparticle suspension viewed from the side by the overview camera. The two electrodes are visible at the top and bottom. The suspension has a central void and it is displaced upward, so that it had only a single layer at the lower void boundary. (c) Single layer imaged by the high-resolution camera. The field of view is indicated in (b) by the yellow rectangle. (enhanced online). (d) Number density of microparticles. This graph indicates that the sample is spatially nonuniform over the entire field of view; consequently, we perform most of our spectral analysis for microparticle data in $0 \leq x \leq 1.62$ mm. [URL: http://dx.doi.org/10.1063/1.3204638.1]

rest at a point in space where the net force is zero. The equilibrium position is on a surface enclosing the plasma center, as sketched in Fig. 2(a).

As we add more microparticles, and they repel one another, they gradually fill space near those equilibrium locations. This leads to a microparticle-free region, called a void, which is surrounded by many microparticles.

C. Single-layer dusty plasma

We observed a microparticle suspension which had only a single layer on the lower boundary of a void. Our focus in this paper is the confinement and oscillatory motion of the microparticles in this single layer. The reason this suspension is not symmetrical, with a single layer at the bottom but many microparticles at the top, is believed to be thermophoresis. The slight downward temperature gradient results in a slight upward thermophoretic force on all microparticles. This shifts the equilibrium forces, so that fewer microparticles are suspended at the bottom.

Single-layer suspensions have been studied in several ground-based experiments, and phenomena that have been observed include compression of a two-dimensional (2D) structure,[8] melting,[6,20] Mach cones,[7] waves and phonon dispersion,[9–11] and transport.[13,18,19,21,22] In these ground-based experiments, the single layer was suspended in the sheath near the lower electrode, with confinement in the vertical direction supplied by a balance of gravity and electric forces.

The single layer studied here differs from those in previous ground-based experiments. Microgravity conditions allow the microparticles to be suspended in the main plasma, where electric fields and ion flow velocities are much weaker than in the sheath. Ion flow is a source of energy for accelerating microparticles in the sheath due to electrostatic fluctuations and disturbances such as the wake effect. Thus, the plasma conditions surrounding our microparticles are less anisotropic and more nearly like equilibrium conditions, as compared to the highly anisotropic and strongly nonequilibrium conditions found in the sheath.

II. APPARATUS

The experiment reported here was performed under microgravity conditions using the PK-3 Plus instrument on the ISS, Fig. 1. We review some features of this instrument here; further details were reported by Thomas *et al.*[27] An advantage of the ISS for performing microgravity experiments is that accelerations are small and observation time can be long. This makes possible experiments, such as the one reported here, which require attaining low velocities under steady-state conditions.

A vacuum chamber contains a pair of parallel-plate electrodes with diameter 6 cm and spacing 3 cm. These electrodes are powered by a 13.56 MHz rf voltage applied symmetrically to the two electrodes, i.e., in a push-pull mode.

Gas is introduced in a brief period termed as "gas cycle." After a few percent overshoot, the gas pressure approaches a steady level within less than a second due to a pressure controller between the chamber and vacuum outlet. The data reported here are for neon gas.

After igniting a plasma, microparticles are injected into the chamber. The microparticles become electrically charged and confined in the plasma. To image the microparticles, they are illuminated by a thin (150 μm) sheet of laser light passing through the chamber. The sheet illuminates an x-z plane, so that a vertical cross section of the microparticle suspension is imaged. The instrument is equipped with video cameras with a resolution of 720 by 576 pixels operated at a frame rate of 25 frames per second.

We used two cameras, the "overview" and "high-resolution" cameras, to image the suspension of microparticles. The high-resolution camera has a magnification of 11.3 μm per pixel in the horizontal direction and 10.3 μm per pixel in the vertical direction, with a field of view of width $L=8.14$ mm. This high-resolution camera offers a sig-

nificant advance over the PK-Nefedov camera because it provides much more magnification. A microparticle fills many pixels, thereby allowing considerable accuracy in measuring its position.

In the video recording, microparticles often appear and then later disappear as they move in and out of the thin sheet of laser light. Some microparticles remained in the laser sheet for hundreds of frames, while others appeared only in a few consecutive frames. Half of the microparticles we observed remained visible for seven consecutive frames or longer. This situation differs from the case of computer simulations, for example, where the same microparticle can be followed throughout the entire period of observation. Therefore, unlike the case of simulations, here we are limited to methods of analysis that do not require long time series for the trajectories of individual microparticles.

The data reported here were recorded during an interval of 63.56 s. During this interval there was no gas inflow because the gas was introduced much earlier. The gas pressure already attained a steady level of 0.12 torr, as measured by a capacitance manometer mounted on the chamber. At this pressure, ion motion is expected to be mobility limited. The rf voltage was 43.8 V peak to peak, the forward rf power was 230 mW, and the rf current was 4.6 mA peak to peak. These rf levels remained steady with no low-frequency modulation applied to the electrodes. The microparticles were 6.81 μm diameter melamine-formaldehyde microspheres with a mass $m_p = 2.5 \times 10^{-13}$ kg. The gas temperature, which was not measured, is expected to be nearly the same as the temperature of the metal components of the chamber, which was measured to be 301 K, with a vertical gradient of 0.047 K/cm between the top and bottom of the chamber due to a slightly higher temperature on the lower electrode, Fig. 1. Using the experimentally measured coefficient[31] $\delta = 1.26 \pm 0.13$ in Eq. (2), we calculate an Epstein damping rate of $\nu_E = 17.6 \pm 1.8\ \mathrm{s}^{-1}$.

Example images of the microparticle suspension are shown in Fig. 2(b) for the overview camera and in Fig. 2(c) for the high-resolution camera recorded simultaneously. The primary data analyzed here are 1590 video frames recorded by the high-resolution camera during the 63.56 s interval. The high-resolution camera was pointed at the left half of the single layer. We note that the single layer is not uniform: it is denser on the left of the images (i.e., near the outer radius of the void) than on the right (below the void's center). Before the images were recorded, two fields separated by 1/50 s were interlaced to form one image. In this experiment, microparticles only occasionally moved faster than 1 mm/s, but when there was such a fast microparticle, it appeared in the final image not as a single bright spot, but rather with a striped pattern that is an artifact of the interlacing.

III. DATA ANALYSIS

A. Particle tracking

Microparticles in the single layer were observed to oscillate in their positions. These oscillations are too small to be observed easily by the eyes when watching the video, but they can be detected and measured using image analysis techniques to track the microparticle motion. Because they moved at very low velocities in this experiment, we used image analysis techniques that have very small errors. Measurement errors are discussed in Appendix A.

Using bitmap images, we identify microparticles as the bright spots in an image like Fig. 2(c). This is done in three steps. First, to reduce artifacts due to interlacing, we smoothed the raw images using a Gaussian blur with a radius of 1 pixel. Second, to identify bright spots, we excluded pixels with grayscale values less than a threshold level. We chose the threshold level as recommended in Ref. 41 to minimize both the signature of pixel-locking effects and any mistaken particle identifications resulting from noise in the image. Third, to identify a bright spot as a microparticle, we required a minimum number of two pixels for the bright spot. Altogether, this particle identification procedure has three adjustable parameters (blur radius, threshold level, and minimum pixels per microparticle); a test of our results for sensitivity to these parameters is presented in Appendix A.

After we identified microparticles as bright spots, we calculate the microparticle's coordinates x,z with subpixel accuracy using the moment method.[41] To reduce pixel-locking effects, each pixel's intensity was adjusted by subtracting a constant pixel value equal to the threshold level.[41]

We then track the microparticle by identifying it in the next video frame and calculating its velocities v_x and v_z as the difference in positions divided by the 0.04 s time between frames. Here, v_z indicates out-of-plane motion, transverse to the layer. From these velocities we calculate the kinetic temperature of the microparticles and the spectra for oscillations.

The microparticle kinetic temperature is calculated separately for the two coordinates as

$$k_B T_x = \langle m_p \tilde{v}_x^2 \rangle, \quad k_B T_z = \langle m_p \tilde{v}_z^2 \rangle, \tag{3}$$

which can be averaged to yield the total kinetic temperature. Here, k_B is Boltzmann's constant, $\tilde{v}_x$ and $\tilde{v}_z$ are the fluctuations of the velocities in the x and z directions, respectively, and $\langle \cdots \rangle$ represents an average over microparticles viewed by the high-resolution camera for the entire 63.56 s interval. This calculation only requires tracking a microparticle for two consecutive frames.

This microparticle kinetic temperature is usually different from the electron temperature, ion temperature, and the internal temperature of the solid material of the microparticles themselves.[22] Therefore, the kinetic temperatures that we report here are not thermodynamic temperatures.

B. Spectral analysis

We performed spectral analysis to detect oscillatory motion within the natural random motion of microparticles. Our method yields two graphs, a wave spectrum (i.e., phonon spectrum) and a power spectrum. We will present the results for transverse oscillations with microparticle motion perpendicular to the single layer. In-plane oscillations also occur, but with a lower frequency that makes their spectrum less interesting, in the presence of significant neutral gas friction.

Motion perpendicular to the single layer has a higher frequency because of the confinement, as discussed in Sec. IV.

The wave spectrum was calculated from a transverse current. This method, using Eq. (B1), requires particle position and velocity data for two consecutive frames, which works well when individual microparticles appear and disappear from the illuminating laser sheet, as they do in this experiment. The resulting wave spectrum characterizes wave energy as function of frequency and wave number. We performed our calculations mainly for the spatial region of $0 \leq x \leq 1.62$ mm, where the number density of microparticles was relatively uniform.

From the wave spectrum, we also calculated a power spectrum for microparticle velocities. This power spectrum is found by integrating the wave spectrum over wave number. Because of the confinement of the single layer, this power spectrum will have a peak at a nonzero frequency. We fit this power spectrum with its peak to two functions: a damped harmonic oscillator driven by white noise, Eq. (B2), and a Lorentzian function equation (B3). These fits yield a measurement of a resonance frequency ω_R. They also yield a measure of the damping rate, which is ν for the harmonic oscillator and a linewidth for the Lorentzian. Further details of our spectral analysis method are presented in Appendix B.

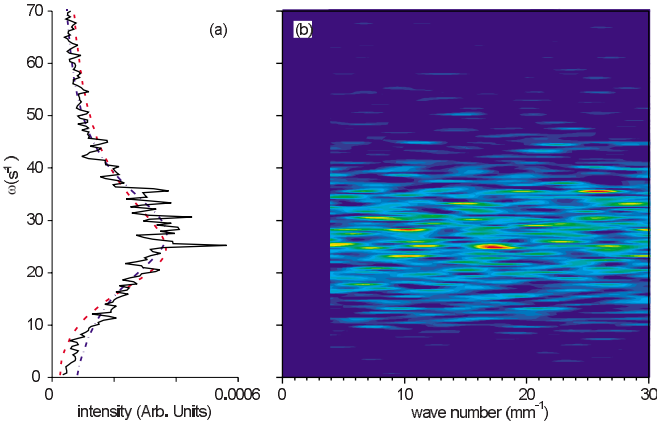

FIG. 3. (Color online) (a) Power spectrum for microparticle velocity fluctuations in the z direction. Microparticle velocities and positions computed by tracking particle motion yield this spectrum. Fits are shown for a theoretical expression for a damped harmonic oscillator driven by white noise (dashed curve) and a Lorentzian (dashed-dotted curve). The central peak indicates the presence of oscillations in the random motion of microparticles and its width indicates damping. The peak is a resonance frequency that we attribute to the confining forces. (b) Wave spectrum with color representing energy (in arbitrary units) as a function of wave number and frequency. The wave frequency does not noticeably vary with wave number, i.e., the wave spectrum lacks the signature of wave dispersion. The power spectrum (a) was computed from the wave spectrum (b) by averaging over k_x.

IV. RESULTS

Our results include five chief observations: the confinement of a single layer, the presence of out-of-plane oscillations, damping of the oscillations, a lack of dispersion that would indicate collective transverse wave motion, and the kinetic temperature of microparticles. We present these results here and discuss their significance in Sec. V.

A. Confinement of a single layer

A confinement of microparticles in a single layer was observed. Within the field of view of the high-resolution camera, there were no microparticles in any other layer during the 63.56 s interval. The number of microparticles visible in the images varied from 14 to 22, as microparticles moved in and out of the illuminating laser sheet. The microparticles were stably confined with small-amplitude motion that appeared to be mostly random.

B. Out-of-plane oscillations

The presence of oscillations in the microparticle motion is revealed by a distinctive peak in the power spectrum of v_z, Fig. 3(a). The peak has a significant linewidth, which we interpret as indicating the damping rate. The power spectrum also has a baseline at a level of about 16% of the peak. We will fit this power spectrum to Eq. (B2) for a damped-driven harmonic oscillator and to Eq. (B3) for a Lorentzian.

The fit for a damped-driven harmonic oscillator yielded a resonance frequency $\omega_R = 25\ \mathrm{s}^{-1}$ and a damping rate $\nu = 24\ \mathrm{s}^{-1}$. The quality of the fit with a correlation coefficient $R^2 = 0.71$ leads us to conclude that the motion in the z direction is adequately described as a damped-driven harmonic oscillator.

The fit to a Lorentzian function yielded a resonance frequency $\omega_R = 27\ \mathrm{s}^{-1}$ and a width $\Delta\omega = 24\ \mathrm{s}^{-1}$. The quality of the fit was characterized by $R^2 = 0.74$.

C. Damping of oscillations

The oscillatory motion is damped at a level that is less than critical damping. The observed damping rate of $24\ \mathrm{s}^{-1}$ is slightly smaller than the resonance frequency of $25\ \mathrm{s}^{-1}$ by a ratio of 0.96. If the motion were critically damped the ratio would be 2. Thus, while the motion is certainly not weakly damped, it can be described as less than critically damped. This damping rate allows a useful comparison to the Epstein damping rate in Sec. V

D. Transverse wave motion

We test for wavelike collective motion by inspecting Fig. 3(b); this inspection reveals no signature of wave dispersion for the transverse motion. If the wave frequency varies with wave number, we would conclude that wavelike motion is present. However, the wave spectrum in Fig. 3(b) is characterized by a frequency band that has little or no dependence on wave number k_x.

E. Kinetic temperature

We calculated the microparticle kinetic temperature using Eq. (3). From our microparticle tracking data for the entire 63.56 s interval, we calculated a total kinetic temperature of 299 K, which is very close to the gas temperature, 301 K. The energy is almost, but not exactly, equally partitioned among two coordinates; the temperature for motion in the in-plane direction $T_x = 312$ K is slightly larger than that for motion in the out-of-plane direction $T_z = 287$ K. (The true

kinetic temperatures for the random motion were probably slightly different from the values reported here because our values include the effects of random errors in the microparticle position measurements.)

V. DISCUSSION

A. Confinement of a single layer

Our first result was the observation of a stable confinement of microparticles in a single layer that was suspended in main plasma. We believe this is the first time that a single layer has been reported to be suspended in the main plasma rather than in (or near) the sheath. This is significant because in the main plasma the conditions are more nearly isotropic and near to equilibrium due to smaller ion flow velocity, as compared to the sheath.

We attribute our observation of a single layer to a confinement in the vertical direction provided by a combination of the ion drag and electric forces, slightly perturbed by a weak upward thermophoretic force. This can be contrasted with the case of single-layer suspensions in ground-based experiments, where vertical confinement is provided by a combination of gravity and the electric force.

B. Out-of-plane oscillations

Our second result was the observation of oscillations of the microparticles perpendicular to the single layer. Observing the oscillations and measuring their resonance frequency are helpful in gaining an understanding of the forces acting on the microparticles, as we discuss next.

The power spectrum that we observed is consistent with a small-amplitude damped-driven harmonic oscillator. In general, harmonic motion is usually the result of conservative forces. Our observation that the oscillation is harmonic is consistent with our prediction, Sec. I A, that the nonconservative aspect of the ion drag force was minimal.

Our measurement for the resonance frequency can be used to estimate the confining forces. Using the observed value $\omega_R = 25\ \mathrm{s}^{-1}$ and calculating $k = m_p \omega_R^2$, we find a force constant of $k = 2.0 \times 10^{-10}\ \mathrm{N\ m}^{-1}$.

We can compare our measurement of the force constant k to measurements in two previous microgravity experiments.[42,43] Our measurement of $k = 2 \times 10^{-10}\ \mathrm{N\ m}^{-1}$ is about an order of magnitude larger than in the previous experiments, which were $k = 0.2\text{–}1.3 \times 10^{-11}\ \mathrm{N\ m}^{-1}$ in Ref. 42 and $k = (1.6 \pm 0.4) \times 10^{-11}\ \mathrm{N\ m}^{-1}$ in Ref. 43. The previous experiments were similar in some ways to ours because they involved video micrography measurements of particle motion in a suspension with a void under microgravity conditions. However, the conditions were not the same. We used neon instead of argon gas and we observed a particle motion within a single layer rather than in a thick multiple-layer region of the suspension. Our method of determining k also differs from those used in previous experiments. We measured the spectrum of microparticle random motion to determine a resonance frequency ω_R, which can be combined with the known microparticle mass to yield k without making any assumptions about an equation of motion or the forces, other than assuming that the net confining force varies linearly with position for small displacements. In the previous experiments k was determined by observing trajectories of microparticles displaced by either some instabilities[42] or laser manipulation,[43] and then performing an analysis using an equation of motion for the microparticles along with some assumptions for the terms in this equation.

We can use the value for the force constant k to estimate the confining forces QE and F_{ID}. These two forces are nearly equal, where they are in balance at the equilibrium position z measured from the midplane of the chamber. (These two forces differ only slightly in magnitude due to the small thermophoretic force.) Using our value of k to estimate these forces requires modeling their dependence on position. We assume, as in Ref. 42, that the electric potential in the void has a parabolic profile, so that E has a linear scaling with z. For the ion drag force, we will consider two limiting cases depending on the ion flow speed v_{ion}. In the low-ion-velocity limit, QE and F_{ID} are both proportional to E, so that their spatial derivatives will contribute equally to k, while at higher v_{ion} approaching the ion thermal speed only the spatial derivative of QE will contribute to k. Thus, in these two limiting cases, we expect $QE = kz/2$ and $QE = kz$, respectively. Using the observed value $z = 7$ mm and our value for k, we estimate that QE is in the range from 5×10^{-13} to 1×10^{-12} N, corresponding to the two limiting case for v_{ion}. We express these values for the force in terms of g, the gravity on Earth's surface: QE and F_{ID} have a magnitude in the range of $0.2\text{–}0.4 m_p g$, where the two values correspond to the two limiting cases for v_{ion}. For comparison, we calculate that the thermophoretic force was two orders of magnitude weaker ($0.005 m_p g$), which validates our assumption that the other two vertical forces acting on the single layer are nearly equal.

The usefulness of performing the experiment under microgravity conditions can be seen not only from a visual inspection of the particle suspension but also by our quantitative estimate of the forces. As has been long known, microgravity experiments allow microparticles to fill an interelectrode region, rather than the sheath region with its higher electric field. Gravity can obscure weaker forces, such as ion drag. Using microgravity conditions allows one to detect (and here, measure) these weaker forces.

C. Damping of oscillations

Our third result, the damping of the oscillations, can be mostly explained by gas friction. We arrive at this conclusion by comparing the fitted value for the damping rate ν to the Epstein damping rate ν_E expected for gas friction. In Sec. II we calculated $\nu_E = 17.6 \pm 1.8\ \mathrm{s}^{-1}$. This value is not greatly smaller than the value $\nu = 24\ \mathrm{s}^{-1}$ from fitting the power spectrum. Other damping mechanisms that have been proposed in the literature[44–47] could have played a role in the experiments, but the agreement of our values of ν and ν_E suggests that they are not significant for the out-of-plane motions of microparticles in the single layer.

D. Transverse wave motion

Our fourth result is the wave spectrum for the out-of-plane transverse motion. Wave dispersion for out-of-plane transverse wave in 2D single-layer dusty plasma has been predicted by simulations[14,48] and theory.[49,50] However, experiments are lacking from the literature. The only previous dusty plasma experiment known to us with out-of-plane transverse waves in a single-layer 2D suspension involved propagation of an externally excited pulsed wave packet.[49] The wave spectrum in Ref. 49 was not experimentally characterized in that experiment. The only experimentally measured dispersion relation, to our knowledge, for out-of-plane transverse wave motion was made not in a 2D layer but in a one-dimensional (1D) chain.[51]

We note that our wave spectrum lacks the signature of wave dispersion that has been predicted previously.[14,48–50] In Fig. 3(b), the frequency of the oscillations does not vary measurably with wave number. This leads to two possible conclusions: either no waves were present at all or waves were present but they were indistinguishable in the wave spectrum.

We can identify three possible reasons for the apparent lack of wave dispersion in the random out-of-plane transverse motion. Wavelike motion could be obscured either by gas damping or nonuniformity in the single-layer suspension, or it might be absent altogether.

The strong damping of microparticle motion can obscure an observation of small effect of wave dispersion. Dispersion, i.e., the range $\delta\omega$ of the frequency as the wave number is varied, can be very small for the out-of-plane transverse wave, especially when the screening of interparticle potential is large.[14,48–50] For example, $\delta\omega$ was only about 4% of the resonance frequency ω_R, as observed in a previous experiment with a 1D chain of microparticles suspended in a sheath at a low gas pressure.[51] In our experiment, however, with a higher gas pressure, the damping rate can result in a linewidth $\Delta\omega$ that is comparable to the ω_R. Thus, dispersion could be too small to detect in our wave spectrum.

Nonuniformity in the microparticle spacing in our experiment could also obscure the wave dispersion due to a natural averaging over different spatial regions. The cause of wave dispersion is interparticle interactions and the strength of these interactions varies with the microparticle spacing. Thus, it is possible that waves could be present but with different frequencies in different regions. To limit this effect in preparing the wave spectrum, Fig. 3(b), we cropped the image to include only $0 \leq x \leq 1.62$ mm. Nevertheless, the remaining nonuniformity could still cause the wave dispersion to be obscured.

Finally, it is possible that transverse wave motion is absent altogether. The possibility that waves are completely lacking might be surprising in the context of plasma physics, where wave motion is usually omnipresent. However, there are examples of physical systems where particles in 2D monolayer systems oscillate as individual oscillators due to a confining out-of-plane potential.[52]

E. Kinetic temperature

Our fifth result was a low value of the observed kinetic temperature. The observed kinetic temperature of 299 K was nearly the same as the 301 K neutral gas temperature, unlike in some other dusty plasma experiments,[53] where the observed kinetic temperature is much larger due to an additional heating mechanism.

Our measurement of the kinetic temperature is significant not only for its numerical value and what it reveals when compared to the gas temperature but also simply because we were able to measure it at all. The literature for previous microgravity dusty-plasma experiments was lacking measurements of kinetic temperature because a high camera resolution was not available in previous space-flight experiments. Here, we exploit the high resolution camera of the PK-3 Plus instrument, which allows us to accurately measure small microparticle velocities, as is required to calculate kinetic temperature. Microgravity experiments have also been reported using parabolic flights of aircraft, but with microgravity conditions that have a higher acceleration level and a shorter duration, which preclude achieving a low kinetic temperature as in our experiment.

The low value of our observed kinetic temperature indicates that Brownian motion due to neutral gas atoms can be the primary energy input for microparticle in the main plasma. This finding was possible because of performing the experiment under microgravity conditions. In ground-based experiments, due to gravity, microparticles are suspended in the sheath where ion flow is strong, providing a source of energy that can result in much higher temperatures. Microgravity conditions allow suspending microparticles in the main plasma where the ion velocity is much slower, providing an environment that is much less anisotropic and more nearly equilibrium.

ACKNOWLEDGMENTS

Work at The University of Iowa was supported by NASA (Grant No. NNX07AD22G). Work in Germany was supported by DLR/BMWi (Grant No. 50WP0203) and by RFBR (Grant No. 06-02-08100). Work in Russia was supported by RFBR (Grant No. 08-02-00444).

APPENDIX A: MEASUREMENT ERROR

1. Tests

Here we present tests of our results for some adjustable parameters in our data analysis. Details of the sources of error in our results are discussed in Appendix A, Sec. A 2.

The spatial region that is included in the analysis is, in general, an adjustable parameter. When the sample is spatially nonuniform, as it is in our experiment, this choice is important because the spectral analysis involves averaging over the included spatial region. We tested our results for the effect of nonuniformity. We found that the fit result for linewidth is 9% larger when we include the entire field of view, as compared to limiting our analysis to the $0 \leq x \leq 1.62$ mm region. This estimate of a 9% effect due to nonuniformities in the entire field of view, while not extremely

serious, is significant enough that we limit our analysis of the spectrum width (Sec. IV) to data in the region $0 \leq x \leq 1.62$ mm.

The threshold level used in identifying particles in the original bitmap images is an adjustable parameter. In a test, we found that varying the threshold level over a factor of two results in no significant effect on the wave spectrum and a slight effect in three of our computed parameters: about 2% effect in kinetic temperature, 1% in resonance frequency, and 7% in damping rate.

2. Sources of error

Our results for the spectrum and temperature reported in Sec. IV are subject to errors that can arise from two sources: the physics assumptions used in fitting the power spectrum and the camera together with the particle measurement analysis methods. Here we discuss these sources of error and the steps we took to minimize them.

a. Physics assumptions

The physics assumptions used in fitting the observed power spectrum to Eq. (B2) could err in at least two ways. First, we assume that the linewidth of the spectrum is entirely due to damping. This ignores the effect of nonuniformity, which could result in averaging spectrum with frequencies that vary according to position, as discussed in Sec. V. Second, we assume a white noise as the driving force that excites the observed particle motion. The assumption that only white noise excites the particle motion appears to be generally reasonable because our observed kinetic temperatures are consistent with Brownian motion arising from collisions with gas atoms. Brownian motion should result in white noise. However, there may also be additional driving mechanisms, such as electrostatic fluctuations in the plasma, that might not be white noise. We have no direct measurements of these fluctuations. If this assumption is in error, the fit parameters that we report, resonance frequency, and linewidth might be in error. We expect that these errors are likely very small because of the agreement of the observed kinetic temperature and the gas temperature.

b. Camera and analysis methods

The camera can introduce errors in two significant ways. First, interlacing can lead to false particle identification for occasional fast microparticles. Second, random errors in pixel values due to electronic noise in the imager can lead to small errors in particle positions and velocities.

False particles identified due to interlacing would account for up to 5% of the total identified particles if we took no countermeasures. To prevent this, in our particle-identification procedure, we first applied a Gaussian blur with a radius of one pixel, and after thresholding the image we applied a requirement of a two-pixel minimum size per particle. These two countermeasures reduced the rate of false particle identifications to less than 0.01%, so that they had no significant effect on our results. Neither of these countermeasures had a significant effect on true particles because most true particles filled at least nine pixels.

Random errors in pixel values due to electronic noise in the imager can lead to errors in the subpixel accuracy of particle position measurements and in the velocities and currents that are computed from the positions. These errors could contribute to the baseline of the power spectrum, Fig. 3(a). To reduce these random errors, we used images from the high-resolution camera so that particles filled more pixels, and in our analysis we used the improved moment method of particle position measurement.[41]

APPENDIX B: SPECTRAL ANALYSIS METHOD

Here we provide details of our method of spectral analysis of microparticle motion. This method was used to find the wave spectrum, power spectrum, and fit results reported in Sec. IV. The method we use was chosen because of the short time series of microparticle velocities that are typical for experiments with 3D suspensions.

In most areas of physics and engineering, calculating a spectrum usually begins with a long time series of data, which is Fourier transformed, yielding a power spectrum. However, this method will not work for our experiment because our measurements do not yield long time series for individual particles. Fortunately, there is a method of calculating a spectrum without tracking particles for more than two consecutive frames; this is the method that begins with calculating a so-called "particle current."[54]

The transverse particle current is computed from the observations of microparticle positions x_i and microparticle velocities $v_{z,i}$ as

$$j_z(k_x,t) = \sum_{i=1} v_{z,i}(t) e^{ik_x x_i(t)}. \tag{B1}$$

This is calculated for a specified wave number k_x. This current is said to be transverse, instead longitudinal, because it uses the z component of particle velocity but the x component of particle position and wave number. In Eq. (B1), $v_{z,i}(t)$ and $x_i(t)$ represent the i^{th} microparticle's velocity and position in the video frame that was recorded at time t. The summation is over all the microparticles in a spatial region we choose. This calculation can be repeated for all video frames in the time interval, which in our experiment was $0 \leq t \leq 63.56$ s. Since the microparticles are not located at the positions of a constant regular lattice, this current can be calculated for any desired wave number k_x larger than $2\pi/L_x$, where L_x is the width of the spatial region we choose.

We calculate the power spectrum of the z-component of the microparticle velocity in two steps. First, we calculate a wave spectrum, which is sometimes called a phonon spectrum.[9] Second, we reduce the information in this wave spectrum to yield a power spectrum, which is a graph of wave energy as a function of only frequency.

The first step, calculating the wave spectrum, is performed using a fast-Fourier transform (FFT) of the current $j_z(k_x,t)$ with respect to time. We repeat this FFT for each specified value of k_x and combine the results of these FFTs to yield a wave spectrum for transverse motion. This is presented as a color contour plot, where color represents a quantity related to microparticle kinetic energy, and the two axes

are wave number k_x and frequency ω. In our experiment, these were calculated for a range of frequency from 0 to 12.5 Hz (and angular frequency from 0 to 78.54 s^{-1}), corresponding to the Nyquist frequency for the camera frame rate. The frame rate was adequate for the small velocities that were observed. In addition to transverse oscillations, longitudinal oscillations could also be characterized using this method of calculating the wave spectrum.

The second step, calculating the power spectrum as a function of frequency only, is done by averaging the wave spectrum (from the first step) over the k_x. This yields the power spectrum as a function of frequency. In our experiment with the transverse wave, this power spectrum had a distinctive peak with a significant linewidth and baseline.

We can fit the power spectrum to two functions. First, anticipating that the microparticles could behave as independent harmonic oscillators that are damped while being driven by a random force, we fit to

$$\frac{k_B T}{m_p \pi} \frac{\nu \omega^2}{(\omega^2 - \omega_R^2)^2 + (\omega \nu)^2} + c. \tag{B2}$$

Equation (B2) is intended for use with a spectrum prepared from velocity data; it is different from the more commonly used expression for position data. It also assumes a broadband random driving force that is white noise, i.e., independent of frequency.[55] Equation (B2) has four fit parameters: the resonance frequency ω_R (which is the same as the peak frequency in the *velocity* power spectrum), damping rate ν, a baseline c, and an amplitude $k_B T/m_p \pi$. Here, T is a temperature characterizing the amplitude of the random force, and it may be different from the kinetic temperature calculated using Eq. (3).

Second, we fit to a Lorentzian

$$\frac{2A}{\pi} \frac{\Delta\omega}{4(\omega - \omega_R)^2 + (\Delta\omega)^2} + c, \tag{B3}$$

which differs from Eq. (B2) in the way that the linewidth $\Delta\omega$ appears. Otherwise, Eqs. (B3) and (B2) have essentially the same kind of fit parameters. The linewidth $\Delta\omega$ is an indication of damping and the area A under the spectrum (excluding the baseline) is an indication of amplitude. For our experiment, this fit to the Lorentzian of Eq. (B3) is merely phenomenological without connection to the underlying physics, unlike the fit to the damped-driven oscillator, Eq. (B2), where the parameters are physically motivated. For example, the damping rate for a damped-driven harmonic oscillator in Eq. (B2) is expected to be the same as the physical friction in the equation of motion for an isolated microparticle.

[1] C. K. Goertz, Rev. Geophys. **27**, 271 DOI:10.1029/RG027i002p00271 (1989).
[2] G. Selwyn, J. McKillop, K. Haller, and J. Wu, J. Vac. Sci. Technol. A **8**, 1726 (1990).
[3] H. Thomas, G. Morfill, V. Demmel, J. Goree, B. Feuerbacher, and D. Möhlmann, Phys. Rev. Lett. **73**, 652 (1994).
[4] J. H. Chu and L. I, Phys. Rev. Lett. **72**, 4009 (1994).
[5] G. J. Kalman, P. Hartmann, Z. Donkó, and M. Rosenberg, Phys. Rev. Lett. **92**, 065001 (2004).
[6] A. Melzer, A. Homann, and A. Piel, Phys. Rev. E **53**, 2757 (1996).
[7] D. Samsonov, J. Goree, Z. W. Ma, A. Bhattacharjee, H. M. Thomas, and G. E. Morfill, Phys. Rev. Lett. **83**, 3649 (1999).
[8] G. A. Hebner, M. E. Riley, D. S. Johnson, P. Ho, and R. J. Buss, Phys. Rev. Lett. **87**, 235001 (2001).
[9] S. Nunomura, J. Goree, S. Hu, X. Wang, A. Bhattacharjee, and K. Avinash, Phys. Rev. Lett. **89**, 035001 (2002).
[10] S. Zhdanov, S. Nunomura, D. Samsonov, and G. Morfill, Phys. Rev. E **68**, 035401(R) (2003).
[11] B. Liu, K. Avinash, and J. Goree, Phys. Rev. Lett. **91**, 255003 (2003).
[12] V. E. Fortov, A. G. Khrapak, S. A. Khrapak, V. I. Molotkov, and O. F. Petrov, Phys. Usp. **47**, 447 (2004).
[13] V. Nosenko and J. Goree, Phys. Rev. Lett. **93**, 155004 (2004).
[14] Z. Donkó, P. Hartmann, and G. J. Kalmann, Phys. Rev. E **69**, 065401(R) (2004).
[15] O. Arp, D. Block, A. Piel, and A. Melzer, Phys. Rev. Lett. **93**, 165004 (2004).
[16] P. Hartmann, G. J. Kalman, Z. Donkó, and K. Kutasi, Phys. Rev. E **72**, 026409 (2005).
[17] V. E. Fortov, O. S. Vaulina, and O. F. Petrov, Plasma Phys. Controlled Fusion **47**, B551 (2005).
[18] S. Ratynskaia, K. Rypdal, C. Knapek, S. Khrapak, A. V. Milovanov, A. Ivlev, J. J. Rasmussen, and G. E. Morfill, Phys. Rev. Lett. **96**, 105010 (2006).
[19] S. Nunomura, D. Samsonov, S. Zhdanov, and G. Morfill, Phys. Rev. Lett. **96**, 015003 (2006).
[20] O. S. Vaulina, I. E. Drangevski, X. G. Adamovich, O. F. Petrov, and V. E. Fortov, Phys. Rev. Lett. **97**, 195001 (2006).
[21] V. Nosenko, S. Zhdanov, A. V. Ivlev, G. Morfill, J. Goree, and A. Piel, Phys. Rev. Lett. **100**, 025003 (2008).
[22] B. Liu and J. Goree, Phys. Rev. Lett. **100**, 055003 (2008).
[23] S. Nunomura, T. Misawa, N. Ohno, and S. Takamura, Phys. Rev. Lett. **83**, 1970 (1999).
[24] G. E. Morfill, H. M. Thomas, U. Konopka, H. Rothermel, M. Zuzic, A. Ivlev, and J. Goree, Phys. Rev. Lett. **83**, 1598 (1999).
[25] V. E. Fortov, A. P. Nefedov, O. S. Vaulina, A. M. Lipaev, V. I. Molotkov, A. A. Samaryan, V. P. Nikitskiĭ, A. I. Ivanov, S. F. Savin, A. V. Kalmykov, A. Ya. Solov'ev, and P. V. Vinogradov, Sov. Phys. JETP **87**, 1087 (1998).
[26] A. P. Nefedov, G. E. Morfill, V. E. Fortov, H. M. Thomas, H. Rothermel, T. Hagl, A. V. Ivlev, M. Zuzic, B. A. Klumov, A. M. Lipaev, V. I. Molotkov, O. F. Petrov, Y. P. Gidzenko, S. K. Krikalev, W. Shepherd, A. I. Ivanov, M. Roth, H. Binnenbruck, J. Goree, and Y. P. Semenov, New J. Phys. **5**, 33.1 (2003).
[27] H. M. Thomas, G. E. Morfill, V. E. Fortov, A. V. Ivlev, V. I. Molotkov, A. M. Lipaev, T. Hagl, H. Rothermel, S. A. Khrapak, R. K. Suetterlin, M. Rubin-Zuzic, O. F. Petrov, V. I. Tokarev, and S. K. Krikalev, New J. Phys. **10**, 033036 (2008).
[28] A. M. Lipaev, S. A. Khrapak, V. I. Molotkov, G. E. Morfill, V. E. Fortov, A. V. Ivlev, H. M. Thomas, A. G. Khrapak, V. N. Naumkin, A. I. Ivanov, S. E. Tretschev, and G. I. Padalka, Phys. Rev. Lett. **98**, 265006 (2007).
[29] A. Piel, M. Klindworth, O. Arp, A. Melzer, and M. Wolter, Phys. Rev. Lett. **97**, 205009 (2006).
[30] P. Epstein, Phys. Rev. **23**, 710 (1924).
[31] B. Liu, J. Goree, V. Nosenko, and L. Boufendi, Phys. Plasmas **10**, 9 (2003).
[32] L. S. Frost, Phys. Rev. **105**, 354 (1957).
[33] M. D. Kilgore, J. E. Daugherty, R. K. Porteous, and D. B. Graves, J. Appl. Phys. **73**, 7195 (1993).
[34] S. A. Khrapak, A. V. Ivlev, G. E. Morfill, and H. M. Thomas, Phys. Rev. E **66**, 046414 (2002).
[35] V. E. Fortov, A. V. Ivlev, S. A. Khrapak, A. G. Khrapak, and G. E. Morfill, Phys. Rep. **421**, 1 (2005).
[36] D. Samsonov and J. Goree, Phys. Rev. E **59**, 1047 (1999).
[37] H. Rothermel, T. Hagl, G. E. Morfill, M. H. Thoma, and H. M. Thomas, Phys. Rev. Lett. **89**, 175001 (2002).
[38] E. Thomas, Jr., B. M. Annaratone, G. E. Morfill, and H. Rothermel, Phys. Rev. E **66**, 016405 (2002).
[39] M. Mikikian, L. Boufendi, A. Bouchoule, H. M. Thomas, G. E. Morfill, A. P. Nefedov, V. E. Fortov, and the PKE-Nefedov team, New J. Phys. **5**, 19 (2003).
[40] V. Land and W. J. Goedheer, New J. Phys. **10**, 123028 (2008).
[41] Y. Feng, J. Goree, and B. Liu, Rev. Sci. Instrum. **78**, 053704 (2007).
[42] M. Kretschmer, S. A. Khrapak, S. K. Zhdanov, H. M. Thomas, and G. E. Morfill, Phys. Rev. E **71**, 056401 (2005).
[43] M. Wolter, A. Melzer, O. Arp, M. Klindworth, and A. Piel, Phys. Plasmas

14, 123707 (2007).
[44]F. Melandsø, T. K. Aslaksen, and O. Havnes, J. Geophys. Res., [Space Phys.] **98**, 13315 DOI:10.1029/93JA00789 (1993).
[45]R. K. Varma, P. K. Shukla, and V. Krishan, Phys. Rev. E **47**, 3612 (1993).
[46]S. V. Vladimirov, Phys. Plasmas **1**, 2762 (1994).
[47]A. V. Ivlev, U. Konopka, and G. Morfill, Phys. Rev. E **62**, 2739 (2000).
[48]K. Qiao and T. W. Hyde, Phys. Rev. E **68**, 046403 (2003).
[49]D. Samsonov, S. Zhdanov, and G. E. Morfill, Phys. Rev. E **71**, 026410 (2005).
[50]S. V. Vladimirov, V. V. Yaroshenko, and G. E. Morfill, Phys. Plasmas **13**, 030703 (2006).
[51]T. Misawa, N. Ohno, K. Asano, M. Sawai, S. Takamura, and P. K. Kaw, Phys. Rev. Lett. **86**, 1219 (2001).
[52]K. D. Gibson and S. J. Sibener, Phys. Rev. Lett. **55**, 1514 (1985).
[53]R. A. Quinn and J. Goree, Phys. Rev. E **61**, 3033 (2000).
[54]J.-P. Hansen and I. R. McDonald, *Theory of Simple Liquids*, 2nd ed. (Elsevier, New York, 1986).
[55]R. Kubo, M. Toda, and N. Hashitsume, *Statistical Physics II: Nonequilibrium Statistical Mechanics* (Springer-Verlag, Berlin, 1985).